Science Bulletin 64 (2019) 1675–1684

Contents lists available at ScienceDirect

Science Bulletin

journal homepage: www.elsevier.com/locate/scib

Science Bulletin
www.scibull.com

Article

Facile self-template fabrication of hierarchical nickel-cobalt phosphide hollow nanoflowers with enhanced hydrogen generation performance

Xupo Liu [a], Shaofeng Deng [a], Peifang Liu [b], Jianing Liang [a], Mingxing Gong [a], Chenglong Lai [a], Yun Lu [a], Tonghui Zhao [a], Deli Wang [a,*]

[a] Key Laboratory of Material Chemistry for Energy Conversion and Storage, Ministry of Education, Hubei Key Laboratory of Material Chemistry and Service Failure, School of Chemistry and Chemical Engineering, Huazhong University of Science and Technology, Wuhan 430074, China
[b] Analysis & Testing Center of Xinyang Normal University, Xinyang 464000, China

ARTICLE INFO

Article history:
Received 10 July 2019
Received in revised form 9 August 2019
Accepted 10 September 2019
Available online 13 September 2019

Keywords:
Self-template method
Hydrolysis of glycerate nanospheres
Kirkendall effect
NiCoP hollow nanoflowers
Hydrogen evolution reaction

ABSTRACT

Developing facile methods to construct hierarchical-structured transition metal phosphides is beneficial for achieving high-efficiency hydrogen evolution catalysts. Herein, a self-template strategy of hydrothermal treatment of solid Ni-Co glycerate nanospheres followed by phosphorization is delivered to synthesize hierarchical NiCoP hollow nanoflowers with ultrathin nanosheet assembly. The microstructure of NiCoP can be availably tailored by adjusting the hydrothermal treatment temperature through affecting the hydrolysis process of Ni-Co glycerate nanospheres and the occurred Kirkendall effect. Benefitting from the promoted exposure of active sites and affluent mass diffusion routes, the HER performance of the NiCoP hollow nanoflowers has been obviously enhanced in contrast with the solid NiCoP nanospheres. The fabricated NiCoP hollow nanoflowers yield the current density of 10 mA cm^{-2} at small overpotentials of 95 and 127 mV in 0.5 mol L^{-1} H_2SO_4 and 1.0 mol L^{-1} KOH solution, respectively. Moreover, the two-electrode alkaline cell assembled with the NiCoP and Ir/C catalysts exhibits sustainable stability for overall water splitting. The work provides a simple but efficient method to regulate the microstructure of transition metal phosphides, which is helpful for achieving high-performance hydrogen evolution catalysts based on solid-state metal alkoxides.

1. Introduction

Hydrogen is considered as the promisingly sustainable and clean energy source to take the place of conventional fossil fuels, which is beneficial for solving the severe energy demand and environmental pollution problems [1–3]. Electrocatalytic hydrogen evolution reaction (HER) is a desirable method to generate high-purity hydrogen from water and has drawn numerous attentions in the last few years [4]. The state-of-the-art electrocatalytic materials for HER are Pt-based precious metal catalysts. However, the high price and scarcity seriously restrict their large-scale applications [5]. Thus, it is urgent to exploit non-noble metal materials with high performance as alternative electrocatalysts [6,7].

During the past decades, transition metal phosphides (TMPs) [8–10], oxides [11–13], chalcogenides [14–16], nitrides [17], and their hybrids [18–20] have been established as electrocatalysts for HER. Among them, TMPs stimulate extensive interests owing to their higher activity, superior chemical stability and lower price [21,22]. Beyond the binary TMPs such as CoP, Ni_2P, FeP, MoP and CuP, ternary NiCoP materials have been intensively researched due to the approximate radii of Ni and Co ions that is beneficial for achieving ternary TMPs instead of metal doped binary TMPs [23]. Hierarchical NiCoP has been confirmed to be one effective strategy to improve electrochemical activity owing to the large exposed surface and affluent mass diffusion routes [24–26]. For instance, porous NiCoP nanowires on nickel foam have been developed and achieved superior HER activity both in alkaline and neutral medium [27]. Ni-Co-P hollow nanobricks with oriented nanosheets have been fabricated by a template-engaged strategy and exhibited high HER activity and stability in alkaline electrolytes [28]. The previous reports revealed that constructing hierarchical structure of NiCoP catalysts can significantly optimize the HER performance. However, the above-mentioned synthesis methods of high-temperature pyrolysis method and hard template-engaged strategy are complicated and difficult to tailor the microstructure availably. Thus, it is indispensable to develop simple and efficient strategy to achieve hierarchical NiCoP.

Solid-state metal alkoxides are a series of compounds that metal ions coordinate with hydroxy groups of polyhydric alcohols

* Corresponding author.
E-mail address: wangdl81125@hust.edu.cn (D. Wang).

https://doi.org/10.1016/j.scib.2019.09.014
2095-9273/

[29]. Compared with small-molecule alkoxides with high moisture sensitivity, solid-state metal alkoxides possess much higher stability towards water, which provides guarantee to regulate their microstructure by controlling the hydrolysis process. The solid-state metal alkoxides can be utilized as self-template to obtain hierarchical precursors of functional oxides and phosphides [30]. In the past few years, the hydrolysis conditions of react time and solution composition are found to have important effect on the hierarchical structure [31–33]. The fabricated materials derived from metal alkoxides always contain ordered nanosheet assembly, high specific area and well-developed porosity, which are favorable for achieving excellent electrocatalytic property [34–36]. Furthermore, it is noted that hydrolysis reaction of alkoxides involves the diffusion process of different ions, which is significantly affected by temperature. However, the influence of hydrothermal temperature on solid-state metal alkoxides is still unknown up to now.

In this work, Ni-Co glycerate nanospheres are selected to study the effect of hydrothermal temperature on the hierarchical structure for the first time. It is found that the microstructure of Ni-Co precursors can be accurately adjusted by just varying the hydrothermal temperatures. After the gas-solid phosphorization, hierarchical NiCoP hollow nanoflowers with ultrathin nanosheet assembly were obtained. The unique hierarchical structure promotes the exposure of active sites and accelerates the mass transport in the electrochemical process. As a consequence, the hierarchical NiCoP displays small overpotentials of 95 and 127 mV in 0.5 mol L^{-1} H_2SO_4 and 1.0 mol L^{-1} KOH solution for HER, respectively, much lower than those of the solid NiCoP nanospheres (157 and 191 mV). The assembled alkaline electrolytic cell assembled with NiCoP-150 and Ir/C catalysts possesses outstanding durability for alkaline overall water splitting. The results confirm that the fabricated hierarchical NiCoP-150 hollow nanoflowers are promisingly utilized as high-performance HER electrocatalysts.

2. Experimental

2.1. Preparation of Ni-Co precursors

Firstly, Ni-Co glycerate nanospheres were prepared through a solvothermal method: 40.5 mg of $Ni(NO_3)_2{\cdot}6H_2O$ and 40.5 mg of $Co(NO_3)_2{\cdot}6H_2O$ were dissolved in 30 mL isopropanol to obtain a transparent solution. Next, 6 mL of glycerol was added in the solution under vigorous magnetic stirring. The obtained solution was poured into a 50 mL autoclave to keep at 160 °C for 6 h. After cooling to room temperature naturally, the product was washed with absolute alcohol for four times and vacuum dried at 60 °C overnight.

To obtain the Ni-Co precursors, the as-prepared Ni-Co glycerate nanospheres were dispersed in 30 mL distilled water for hydrothermal treatment at a certain temperature. Three samples were treated at 20, 50 and 80 °C for 5 h in a glass bottle with magnetic stirring, which are denoted as NiCoG-20, NiCoG-50 and NiCoG-80, respectively. Meanwhile, another four samples were poured into a 50 mL autoclave and treated at 115, 150, 185 and 220 °C for 5 h, denoted as NiCoG-115, NiCoG-150, NiCoG-185 and NiCoG-220, respectively. The products were washed with vast absolute alcohol for several times and then dried in vacuum at 60 °C for 12 h. In addition, the Ni-Co glycerate nanospheres without any treatment (denoted as NiCoG-N) were also applied for comparison.

2.2. Synthesis of NiCoP catalysts

The gas-solid phosphating method was utilized to synthesize NiCoP. Generally, two porcelain boats containing the Ni-Co precursor (30 mg) and $NaH_2PO_2{\cdot}H_2O$ (300 mg) were placed downstream and upstream of the tube furnace, respectively. Next, the sample was heated up to 300 °C at 2 °C min^{-1} and maintains for 2 h in Ar atmosphere. The final phosphides were obtained after cooling down to room temperature. The phosphides derived from NiCoG-N, NiCoG-80, NiCoG-150 and NiCoG-220 were denoted as NiCoP-N, NiCoP-80, NiCoP-150 and NiCoP-220, respectively.

2.3. Characterization

Microscopic images were determined by the field emission scanning electron microscope (SEM, Sirion200) and transmission electron microscope (TEM, Tecnai G2 F20). X-ray diffraction (XRD) spectra were determined by the X'Pert PRO diffractometer. Thermogravimetric analysis (TGA) was obtained on a TA Q500 instrument ranging from 30 to 600 °C with a heating rate of 10 °C min^{-1} in air. The Fourier transform infrared spectra (FTIR) were tested by a FTIR spectrometer (VERTEX 70). The thickness of nanosheets was recorded by a Thermal iCE 3000 atomic force microscope (AFM). The specific surface areas were conducted on an ASAP2420-4MP analyzer after the samples were degassed at 200 °C under vacuum overnight. X-ray photoelectron spectroscopy (XPS) data was collected using an AXIS-Ultra DLD-600W instrument and all the XPS spectra were calibrated based on the C 1s peak of 284.8 eV.

2.4. Electrochemical measurements

A three-electrode system was applied to evaluate the electrochemical performances of the as-prepared catalysts by utilizing an Autolab PG302N electrochemical workstation. The glassy carbon electrode was utilized as the working electrode, while the graphite rod and reversible hydrogen electrodes were chosen as the counter and reference electrodes, respectively. A 32 μL of the resultant catalyst slurry (1 mL 0.1% Nafion isopropyl/alcohol mixed solution and 5 mg catalyst) was dispersed on the glassy carbon to prepare the working electrode with a loading amount of 0.8 mg cm^{-2}. For the HER measurements, linear sweep voltammetry (LSV) were determined in 1.0 mol L^{-1} KOH or 0.5 mol L^{-1} H_2SO_4 media with the potential from 0.2 to −0.4 V at a scan rate of 5 mV s^{-1}. The cyclic voltammetry (CV) tests were performed to estimate the electrochemically active surface area (ESCA) at scanning rates of 20, 40, 60, 80, 100 and 120 mV s^{-1} with the potential range of 0.1–0.3 V. To obtain the stability, continuous CV was performed for 3000 circles ranging from −0.1 to 0.1 V at the scan rate of 100 mV s^{-1}. The chronoamperometry curve of HER was also recorded with a fixed current density of 10 mA cm^{-2} for 24 h at a rotation speed of 1600 r min^{-1}. Otherwise, a two-electrode system was carried out for overall water splitting in 1.0 mol L^{-1} KOH. The cathode and anode were fabricated by dispersing the NiCoP-150 and self-made 20% Ir/C on 1 cm × 1 cm carbon cloth substrates with the loading amount of 2 mg cm^{-2}, respectively. The chronopotentiometry curve was applied to estimate the overall water splitting performance at a constant current density of 10 mA cm^{-2}. In this work, all the electrochemical results were analyzed without the iR compensation.

3. Results and discussion

3.1. Temperature-regulated morphology evolution of Ni-Co precursors

Scheme 1 illustrates the general concept of synthesizing the hierarchical Ni-Co precursors (hollow nanoflowers) by hydrothermal treatment of the Ni-Co glycerate nanospheres. Firstly, Ni-Co glycerate nanospheres (NiCoG-N) were prepared through the solvothermal method. The ions of Ni^{2+} and Co^{2+} replace the H^+ of

hydroxyl groups in glycerol to generate uniform Ni-Co glycerate nanospheres with the average diameter of 500 nm (Fig. S1 online) [30,37]. The TGA result in Fig. S2 (online) shows a large weight loss of 45.2% occurred from 150 to 285 °C because of the dissociation of organic components in Ni-Co glycerate. Secondly, the Ni-Co glycerate nanospheres were converted into the Ni-Co precursors by the hydrothermal method. Hydrothermal temperatures ranging from 20 to 220 °C are systemically investigated to tailor the morphologies of Ni-Co precursors. Fig. S3 (online) depicts the optical photographs of the Ni-Co precursors at different temperatures and it is clearly noted that the samples present different colors, implying the various structures and phase compositions. To achieve the influence of hydrothermal temperature on Ni-Co precursors, the morphologies were determined and presented in Fig. 1a–h. It can be observed that the Ni-Co glycerate nanospheres (NiCoG-N) contain a smooth surface (Fig. 1a). With gradually increasing the hydrothermal temperature, the surface of nanospheres become rough and some nanosheets appear on the surface of nanospheres (Fig. 1b–f), which is attributed to the hydrolysis reaction of Ni-Co glycerate nanospheres to produce hydroxide nanosheets [31]. The hydroxyl groups in water react with metal ions of Ni^{2+} and Co^{2+} to form the flake-like hydroxide on the surface. The elevated temperature is beneficial for enhancing the ion diffusion, resulting in faster hydrolysis reaction process. The sphere structure can be maintained until the temperature increases up to 150 °C (Fig. 1f). However, the nanospheres collapse and convert into small nanosheets when the hydrothermal temperature reaches 185 °C (NiCoP-185) and 220 °C (NiCoP-220) as shown in Fig. 1g, h. The reason why the nanospheres collapse will be discussed combining with the TEM analysis below.

The XRD patterns of four represented precursors, NiCoG-N, NiCoG-80, NiCoG-150 and NiCoG-220, were selected to determine the phase compositions of Ni-Co precursors. As shown in Fig. S4a (online), there is a low-angle characteristic peak at around 10.4° in the pattern of NiCoG-N, which is corresponding to the lamellar structure of Ni-Co glycerate [32]. The precursors of NiCoG-80 and NiCoG-150 display three weak peaks located at 18.4°, 33.6° and 60.1°, corresponding to the structures of $Ni_2(OH)_2CO_3{\cdot}4H_2O$ (PDF-38-0714) and $Co(CO_3)_{0.5}OH{\cdot}0.11H_2O$ (PDF-48-0083). The carbonate groups (CO_3^{2-}) are resulting from the decomposition of glycerinum and the similar results have also been reported in previous work [33,38]. In addition, as the continuously increasing temperature, NiCoG-220 shows obvious diffraction peaks belonging to the phases of $Ni(OH)_2$ (PDF-74-2075) and $Co(OH)_2$ (PDF-74-1057). The XRD results indicate that the Ni-Co glycerate undergoes the phase transformation from subcarbonates to hydroxides as the temperature increases. The FTIR spectra in Fig. S4b (online) were also carried out to identify the structure of these precursors. The characteristic peaks are mainly attributed to the metal-O-C (stretching vibration, 596 cm^{-1}), C–H (bending vibration, 806, 1417 cm^{-1}), C–O (stretching vibration, 1001, 1055, 1113, and 1655 cm^{-1}) and C–C (stretching vibration, 1589 cm^{-1}) groups of Ni-Co glycerate [31,39]. These peaks gradually disappear owing to the consumption of Ni-Co glycerate as the temperature increases. However, a new peak appeared at 1615 cm^{-1}, which is corresponding to hydroxyl groups of the formed hydroxide [40].

For better understanding the evolution of Ni-Co glycerate nanospheres, the TEM images of NiCoG-N, NiCoG-80, NiCoG-150 and NiCoG-220 were recorded in Figs. 1i–l and S5 (online). Figs. 1i and S5a (online) display the solid sphere morphologies of NiCoG-N. After hydrothermal treatment at 80 °C for 5 h, it is found that NiCoG-80 shows solid sphere morphology with many thin nanosheets on the surface (Figs. 1j and S5b (online)). When the hydrothermal temperature increases to 150 °C, NiCoG-150 displays a unique hierarchical structure of hollow nanospheres with self-assembly nanosheets (hollow nanoflowers) in Figs. 1k and S5c (online). The formation of peculiar hollow structure is on account of the Kirkendall effect as shown in Scheme 1 [41–43]. It is known that the Kirkendall effect occurs when the diffusion rate of cores is more quick than that of shells, which is significantly affected by the temperature [44]. By comparing the morphologies of NiCoP-80 (solid + nanosheets) and NiCoP-150 (hollow + nanosheets), it can be noted that much larger difference of diffusion rates between outer subcarbonate shells and internal glycerate cores is obtained at 150 than 80 °C, which is indispensable for the formation of hollow structure. When the temperature is at 80 °C, the difference of diffusion rates of subcarbonate shells and glycerate cores is little, leading to fabricate solid spheres with outer nanosheets. When the temperature increases to 150 °C, the diffusion rate of internal metal glycerates is faster than that of outer subcarbonate shells, resulting in the generation of hollow structure [45]. As the hydrothermal temperature is raised to 220 °C, the nanospheres completely disappear and only some nanosheets are found (Figs. 1l and S5d (online)). The reason for the collapse of sphere structure can be concluded as follows: the higher hydrothermal temperature of 220 °C leads to produce much larger pressure in

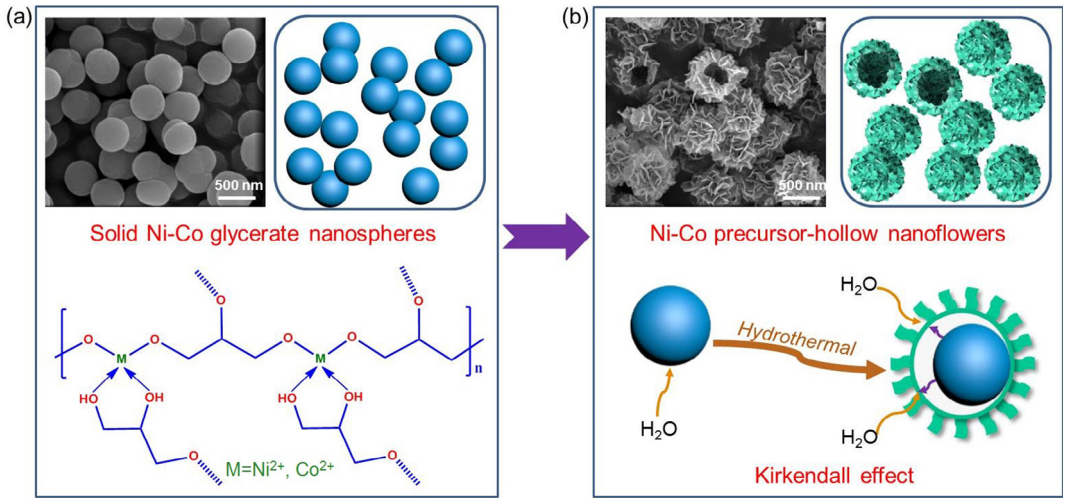

Scheme 1. (Color online) Schematic illustration of preparing hierarchical Ni-Co precursors (hollow nanoflowers) by hydrothermal treatment of solid Ni-Co glycerate nanospheres. (a) The morphology and supposed structure of Ni-Co glycerate. (b) The morphology of Ni-Co precursor and illustration of Kirkendall effect.

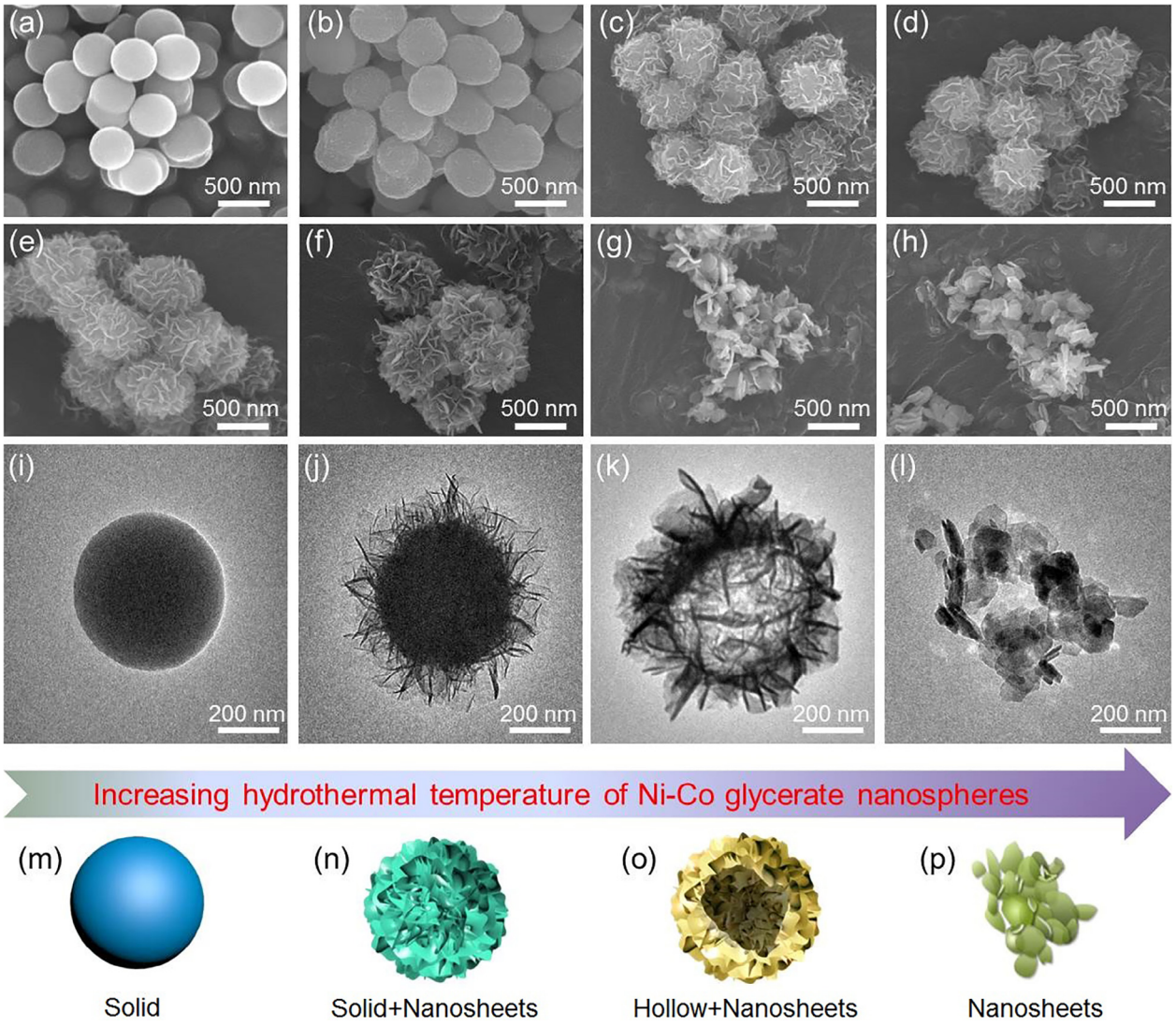

Fig. 1. (Color online) SEM images of Ni-Co precursors: (a) NiCoG-N, (b) NiCoG-20, (c) NiCoG-50, (d) NiCoG-80, (e) NiCoG-115, (f) NiCoG-150, (g) NiCoG-185, and (h) NiCoG-220. TEM images of Ni-Co precursors: (i) NiCoG-N, (j) NiCoG-80, (k) NiCoG-150, and (l) NiCoG-220; the corresponding schematic illustrations of samples: (m) NiCoG-N, (n) NiCoG-80, (o) NiCoG-150 and (p) NiCoG-220.

the autoclave and the hollow structure is not stable in such high-pressure condition. It is interesting to observe the collapse phenomenon of hollow nanospheres in hydrothermal condition, which is seldom reported in the studying of metal alkoxides. This evolution process occurs in a typical "self-template" manner, in which the original Ni-Co glycerate nanospheres function not only as a template, but also as a precursor for the nanosheet formation. Fig. 1m–p simulates the structure transformation of Ni-Co glycerate nanospheres as the hydrothermal temperature increases, revealing that the structure of Ni-Co precursors can be availably tailored by adjusting the hydrothermal temperature.

3.2. Synthesis and characterization of hierarchical NiCoP

Among these precursors, the four representative samples with quite different morphologies, NiCoG-N, NiCoG-80, NiCoG-150 and NiCoG-220, were selected to prepare the NiCoP catalysts by the gas-solid phosphorization method. Fig. 2a–d shows the morphologies of the as-prepared NiCoP-N, NiCoP-80, NiCoP-150 and NiCoP-220 catalysts, respectively. It can be observed that all the phosphides remain the original morphologies of Ni-Co precursors. The XRD pattern of NiCoP-150 in Fig. 2h is readily indexed to the structure of NiCoP (PDF-71-2336). A close observation of the TEM images in Fig. 2e–g reveals that the NiCoP-150 nanoflowers possess hollow structure with average sizes of 630 nm and self-assembly nanosheets on the surface. The peculiar configuration of hollow nanoflowers can validly render the occurrence of nanosheet aggregation during the electrocatalytic process. The average thickness of the nanosheets was detected to be 3.5 nm by AFM in Fig. S6 (online). According to the previous paper [46], the thickness of ultrathin two-dimensional nanomaterials is typically less than 5 nm. Therefore, the as-prepared hierarchical NiCoP reveals an ultrathin nanosheet structure. The ultrathin nanosheets are advantageous to promote the exposure of active sites. Furthermore, the Brunauer-Emmett-Teller (BET) specific surface area of the NiCoP-150 catalyst is recorded to be 41.5 $m^2 g^{-1}$, which is almost three times larger than that of NiCoP-N (10.5 $m^2 g^{-1}$) (Fig. S7 online). It indicates that the specific surface area of NiCoP has been obviously improved through the effective morphology regulation. In addition, the energy-dispersive X-ray spectroscopy (EDX) mapping images (Fig. 2i–l) confirm the presence of Ni, Co and P elements in NiCoP-150. The high-resolution TEM images in

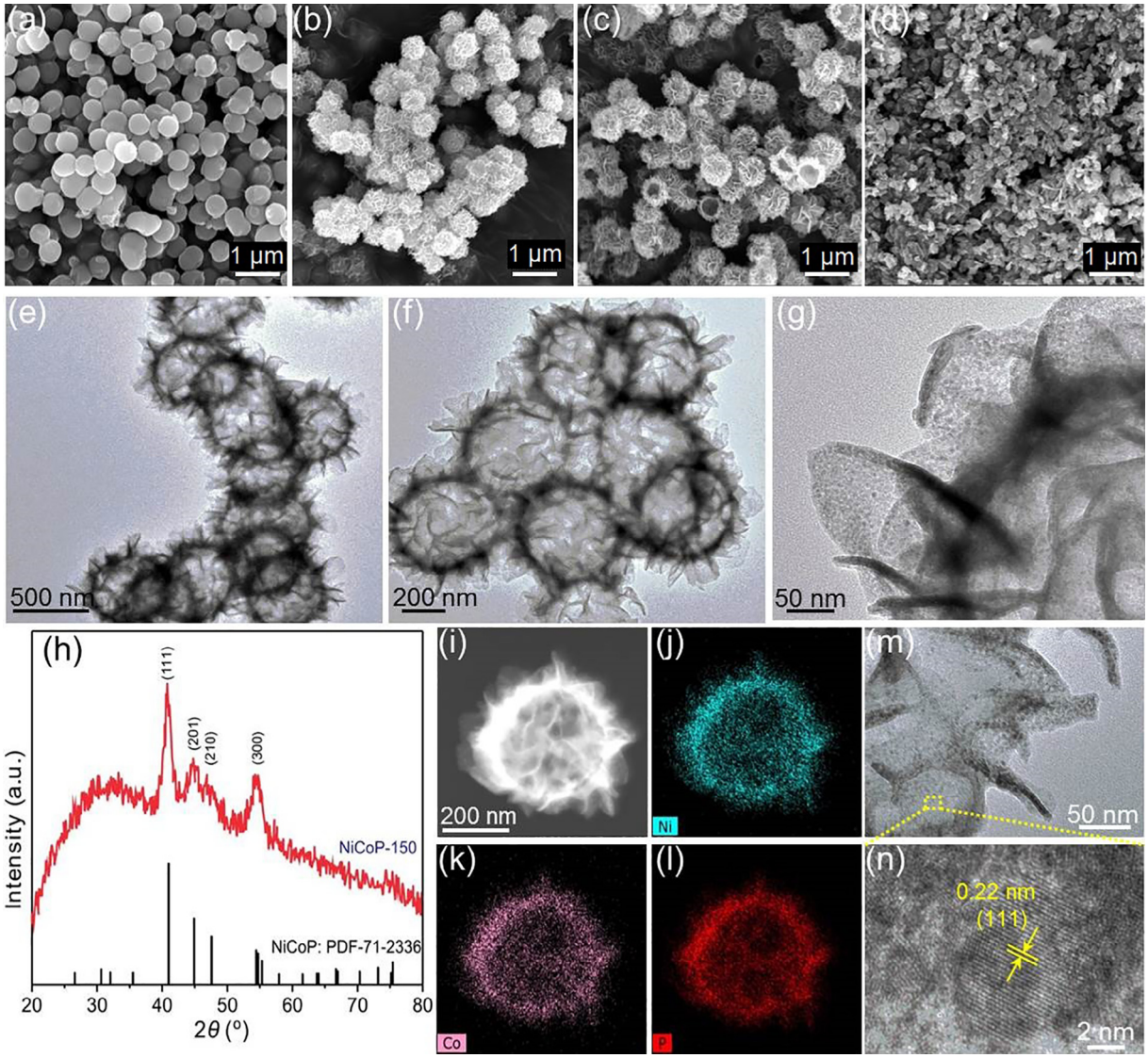

Fig. 2. (Color online) SEM images of hierarchical phosphides: (a) NiCoP-N, (b) NiCoP-80, (c) NiCoP-150 and (d) NiCoP-220; (e–g) TEM images of NiCoP-150 with different resolution; (h) XRD pattern of NiCoP-150 and the standard diffraction image of NiCoP; (i–l) EDX elemental mapping images of NiCoP-150; (m), (n) high-resolution TEM images of hierarchical NiCoP-150.

Fig. 2m, n shows that NiCoP-150 possesses an lattice distance of 0.22 nm, belonging to the (1 1 1) lattice plane of NiCoP [27]. Above all, the results indicate that the hierarchical NiCoP catalyst with high specific surface area is successfully synthesized.

XPS analysis was applied to investigate the surface component and electronic structure of NiCoP-150. The survey spectra in Fig. 3a prove the existence of Ni, Co, and P, which is corresponding to the elemental mapping results in Fig. 2i–l. Fig. 3b displays the high-resolution Ni 2p spectrum of NiCoP-150. It is clearly noted that the characteristic peaks at 856.4 and 874.5 eV belongs to Ni $2p_{3/2}$ and Ni $2p_{1/2}$ of oxidized Ni species with two shake-up satellites located at 860.8 and 879.9 eV. In addition, the peak at around 852.6 eV is ascribed to $Ni^{\delta+}$ species in NiCoP-150 (the value of δ is approximate to be zero) [23]. In the Co 2p spectrum (Fig. 3c), the peaks of 781.3 and 778.0 eV along with one satellite peak of 784.9 eV are attributed to Co $2p_{3/2}$, while the peaks of 797.8 and 793.1 eV as well as one satellite peak of 803.5 eV are attributed to Co$2p_{1/2}$ [32,47]. Otherwise, in the P 2p region of NiCoP-150 (Fig. 3d), the peak of 133.8 eV is attributed to the generated oxidized P species (PO_4^{3-}) because of the exposure of NiCoP in air [48,49]. The peaks of 128.9 and 129.7 eV belong to P $2p_{3/2}$ and P $2p_{1/2}$ of $P^{\delta-}$ in the type of metal phosphides, indicating a negative shift from the elemental P (130.2 eV) [50]. The negative shift of P indicates that the electron density is transferred from Ni and Co to P in the NiCoP catalyst. As a consequence, P sites act as proton-acceptor sites and metal sites act as hydride-acceptor sites, leading to high activity of NiCoP for hydrogen evolution process [24]. Recent works [51,52] have demonstrated that PO_4^{3-} species are beneficial for facilitating water molecule adsorption and promoting oxidation of metal ions for the proton coupled electron transfer procedure. Therefore, the PO_4^{3-} species on the surface can promote the HER process. Moreover, the amount of PO_4^{3-} species on the surface is very small, so they can be detected by the XPS spectra not by XRD technique. Therefore, we think that the produced PO_4^{3-} species can promote the HER process, but the effect may be slight due to the inferior HER performance and small amount of phosphates. The active sites of the as-prepared catalysts are mainly attributed to the NiCoP phases. The as-prepared NiCoP catalyst is expected to have enhanced HER performance.

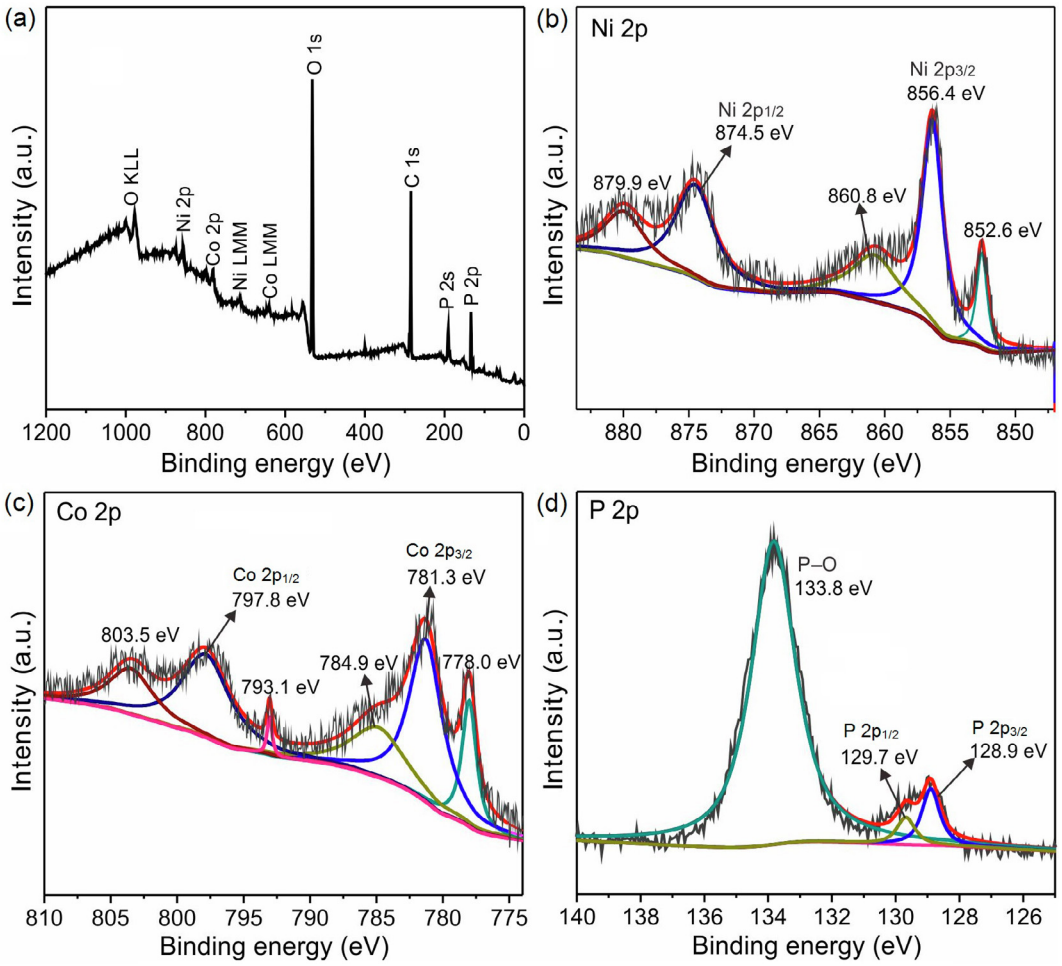

Fig. 3. (Color online) (a) XPS survey spectrum of NiCoP-150; high-resolution spectra of Ni 2p (b), Co 2p (c) and P 2p (d) for NiCoP-150.

3.3. HER performances of NiCoP

HER performances of the synthesized NiCoP catalysts were investigated via the LSV determination. Fig. 4a compares the HER polarization curves of the different glass carbon electrodes modified with NiCoP-N, NiCoP-80, NiCoP-150, NiCoP-220 and Pt/C in 0.5 mol L^{-1} H_2SO_4. The benchmark Pt/C displays the best HER performance and it needs an overpotential of 28 mV to obtain the current density of 10 mA cm^{-2}. It can be observed that the NiCoP catalysts with different morphologies exhibit diverse electrochemical performances. Notably, NiCoP-150 requires a small overpotential of 95 mV to gain the current density of 10 mA cm^{-2}, which is much lower than those of NiCoP-N (157 mV), NiCoP-80 (109 mV) and NiCoP-220 (126 mV). Compared with the solid NiCoP nanospheres (NiCoP-N), the excellent HER property of hollow NiCoP nanoflowers (NiCoP-150) suggests that the formation of hierarchical structure is of importance for enhancing the electrochemical performance of HER. The performances of NiCoP-150 in acidic condition outperform many transition metal phosphide catalysts in the recently published works (Table S1 online). Specially, the HER overpotential of NiCoP-220 is much higher compared to that of NiCoP-150 due to the aggregation of the collapsed nanosheets. Fig. 4b shows the Tafel plots acquired from the corresponding HER polarization curves. The calculated Tafel slope of the Pt/C catalyst is 32 mV dec^{-1}, in good accordance with the literature report [53]. NiCoP-150 exhibits a Tafel slope of 63 mV dec^{-1}, which is much smaller than those of NiCoP-N (102 mV dec^{-1}), NiCoP-80 (69 mV dec^{-1}) and NiCoP-220 (74 mV dec^{-1}), indicating a fast HER kinetics. The Tafel slopes of the as-prepared catalysts fall in the scope of 60–120 mV dec^{-1}, suggesting a Volmer-Heyrovsky mechanism ($H^+ + e^- = H_{ads}$, $H^+ + e^- + H_{ads} = H_2$) [54]. The HER performances of NiCoP-150 with the loading amounts of 0.3 and 0.8 mg cm^{-2} were also determined as shown in Fig. S8a and c (online). It is found that the difference value of 11 mV is obtained for the overpotential at 10 mA cm^{-2} and the corresponding Tafel value only has a difference of 5 mV dec^{-1} in 0.5 mol L^{-1} H_2SO_4 solution. The effect of loading amounts on the HER performances in this work is slight. Moreover, the high loading amount does not increase the cost of water splitting application due to the low price of non-precious metal catalysts. To deep understand the HER activity of the catalysts, the double-layer capacitance (C_{dl}) that was obtained from the CV curves (Fig. S9 online) is applied to evaluate the relative electrochemical surface areas (ECSA). Generally, C_{dl} is proportional to the ECSA value and always applied as one descriptor for ECSA. Fig. 4c indicates that the C_{dl} of NiCoP-150 (2.27 mF cm^{-2}) is much larger than those of NiCoP-N (0.36 mF cm^{-2}), NiCoP-80 (1.47 mF cm^{-2}) and NiCoP-220 (0.72 mF cm^{-2}). The high C_{dl} value of NiCoP-150 can be attributed to the hollow nanoflower structure and the exposed active sites, leading to the enhanced HER performance.

Alkaline water splitting is the widely used method to produce high-purity hydrogen and remarkable alkaline HER performance is also significant for HER catalysts [55]. The HER performance of these samples were also determined in alkaline media. Fig. 4d

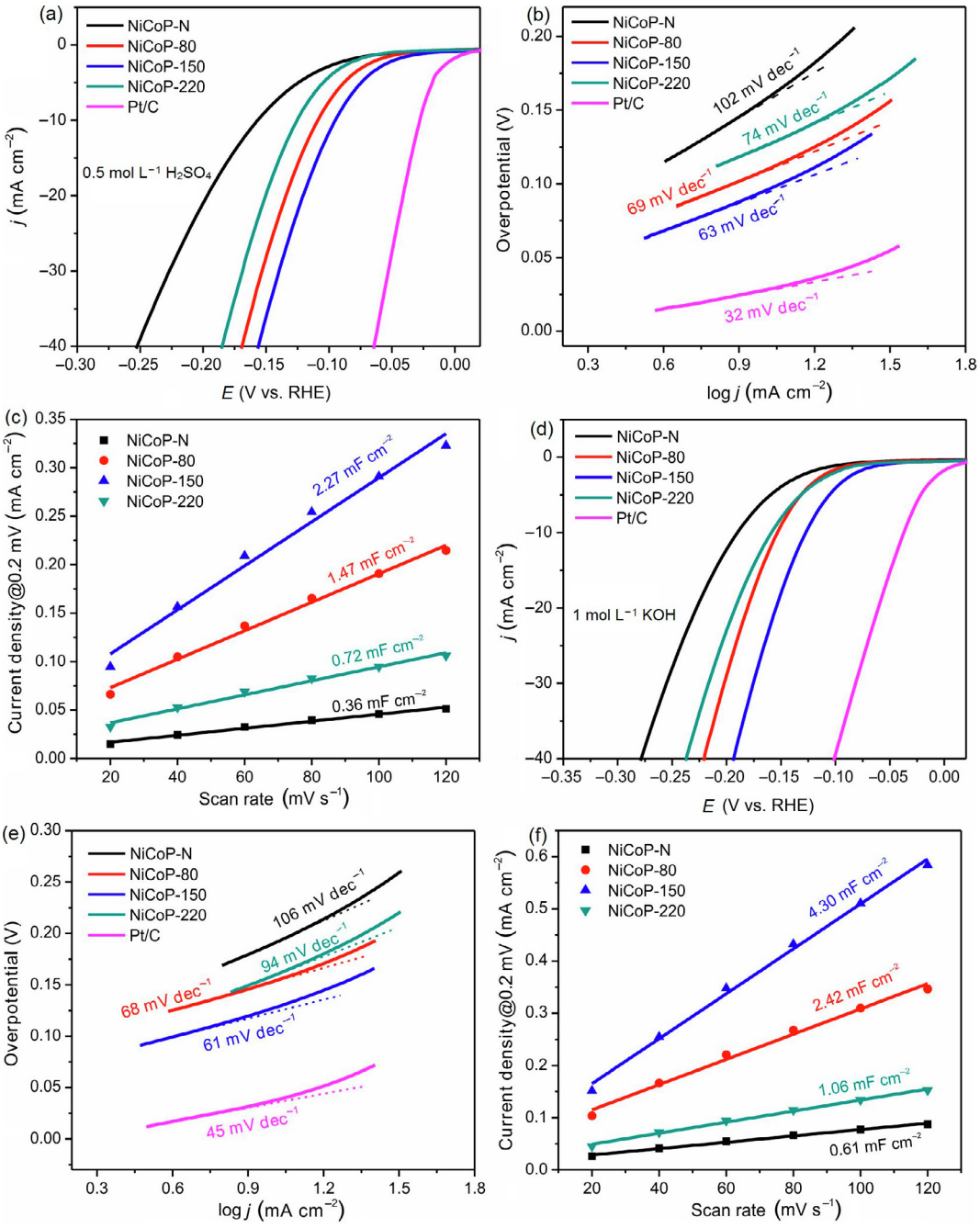

Fig. 4. (Color online) (a) Polarization curves of NiCoP-N, NiCoP-80, NiCoP-150, NiCoP-220 and Pt/C in 0.5 mol L^{-1} H_2SO_4; (b) corresponding Tafel plots of polarization curves with linear fittings; (c) scan rate dependence of the current densities at 0.2 V. (d) Polarization curves of NiCoP-N, NiCoP-80, NiCoP-150, NiCoP-220 and Pt/C in 1.0 mol L^{-1} KOH; (e) corresponding Tafel plots of polarization curves with linear fittings; (f) scan rate dependence of the current densities at 0.2 V.

depicts the polarization curves of NiCoP-N, NiCoP-80, NiCoP-150, NiCoP-220 and Pt/C in 1.0 mol L^{-1} KOH. Obviously, the benchmark Pt/C still exhibits the optimal HER activity with an overpotential of 37 mV to achieve the current density of 10 mA cm^{-2}. The NiCoP-N catalyst composed with solid nanospheres delivers relatively poor HER activity with a high overpotential of 191 mV to deliver a current density of 10 mA cm^{-2}. However, the HER performance has been remarkably improved for the samples with hydrothermal treatment. Obviously, to drive the current density of 10 mA cm^{-2}, NiCoP-150 shows a low overpotential of 127 mV, which is superior to those of NiCoP-N (191 mV), NiCoP-80 (153 mV) and NiCoP-220 (159 mV). The excellent HER performance of NiCoP-150 in alkaline solution is superior to those of many reported phosphide catalysts (Table S2 online). In addition, the Tafel slope of NiCoP-150 is determined to be 61 mV dec^{-1} (Fig. 4e), a little higher than that of Pt/C (45 mV dec^{-1}), but much lower than those of the NiCoP-N (106 mV dec^{-1}), NiCoP-80 (68 mV dec^{-1}) and NiCoP-220 (94 mV dec^{-1}), revealing a Volmer-Heyrovsky mechanism in alkaline media ($H_2O + e^- = H_{ads} + OH^-$, $H_2O + e^- + H_{ads} = H_2 + OH^-$) [56]. The Volmer reaction is the main rate-determining step for all the NiCoP catalysts, while NiCoP-150 follows a faster Volmer-Heyrovsky mechanism than other NiCoP samples. For comparison, the HER properties of NiCoP-150 with the different loading amounts of 0.3 and 0.8 mg cm^{-2} were also detected as shown in Fig. S8b and d (online). It is found that the slight effect of loading amount is obtained for the NiCoP-150 catalyst. Furthermore, the

C_{dl} values of these samples were also calculated to estimate the ECSA according to the CV curves (Fig. S10 online). As shown in Fig. 4f, the C_{dl} values of NiCoP-N, NiCoP-80, NiCoP-150 and NiCoP-220 are 0.61, 2.42, 4.30 and 1.06 mF cm^{-2}, respectively, which are consistent to those in 0.5 mol L^{-1} H_2SO_4.

The HER performances of NiCoP catalysts with different microstructures have been systematically investigated in acid and alkaline electrolytes. It is noted that the HER property is closely related to the corresponding microstructures. The hierarchical NiCoP hollow nanoflowers (NiCoP-150) show superior HER performances compared to the samples of solid nanospheres (NiCoP-N), solid nanospheres with nanosheets (NiCoP-80) and nanosheets (NiCoP-220). The excellent HER property of NiCoP-150 can be ascribed to the following reasons: (i) the hollow structure and ultrathin nanosheets produce high specific surface area, which is beneficial for promoting the exposure of active sites; (ii) the self-assembly sphere configuration can effectively prevent the aggregation of ultrathin nanosheets in the electrocatalytic process, which is advantageous to the fast mass transport. Thus, the available microstructure regulation can achieve the goal of optimizing the HER performance of NiCoP catalysts.

3.4. Stability and water splitting

Stability is another important parameter of HER catalysts for practical application. Firstly, the continuous CV cycling was applied to evaluate the stability of NiCoP-150 catalyst. As depicted in Fig. 5a and b, the polarization curves after 3000 CV cycles show negligible decay compared to the initial ones in 0.5 mol L^{-1} H_2SO_4 and 1 mol L^{-1} KOH solutions, respectively. Furthermore, the chronoamperometry responses in 0.5 mol L^{-1} H_2SO_4 and 1 mol L^{-1} KOH solutions were also determined to estimate the HER stability of NiCoP-150. The current density only shows a small decay after operating for 24 h, revealing excellent stability of NiCoP-150. Considering the outstanding activity and stability of NiCoP-150, the two-electrode cell is assembled with NiCoP-150 and 20% Ir/C catalysts for overall water splitting. Fig. 5c displays the chronopotentiometry curve of the cell in 1 mol L^{-1} KOH solution. It just requires a cell voltage of 1.66 V to drive the current density of 10 mA cm^{-2} and continuously maintains for 24 h. The long-time durability determination confirms the apparent advantage of the hierarchical NiCoP-150 as a high-performance HER electrocatalyst.

4. Conclusions

In summary, we employed a facile self-template strategy to prepare hierarchical NiCoP hollow nanoflowers. The effect of hydrothermal treatment temperature on Ni-Co glycerate spheres has been systematically investigated. It is found that the hydrolysis process of Ni-Co glycerate spheres can be significantly enhanced to produce flake-like hydroxide as the increasing temperature, which provides the guarantee for availably tailoring the nanoscale morphology of NiCoP. The Kirkendall effect is also observed to form hollow structure due to the different diffusion rates of outer subcarbonate shells and internal glycerate cores. After the subsequent phosphorization treatment, hollow NiCoP nanoflowers with

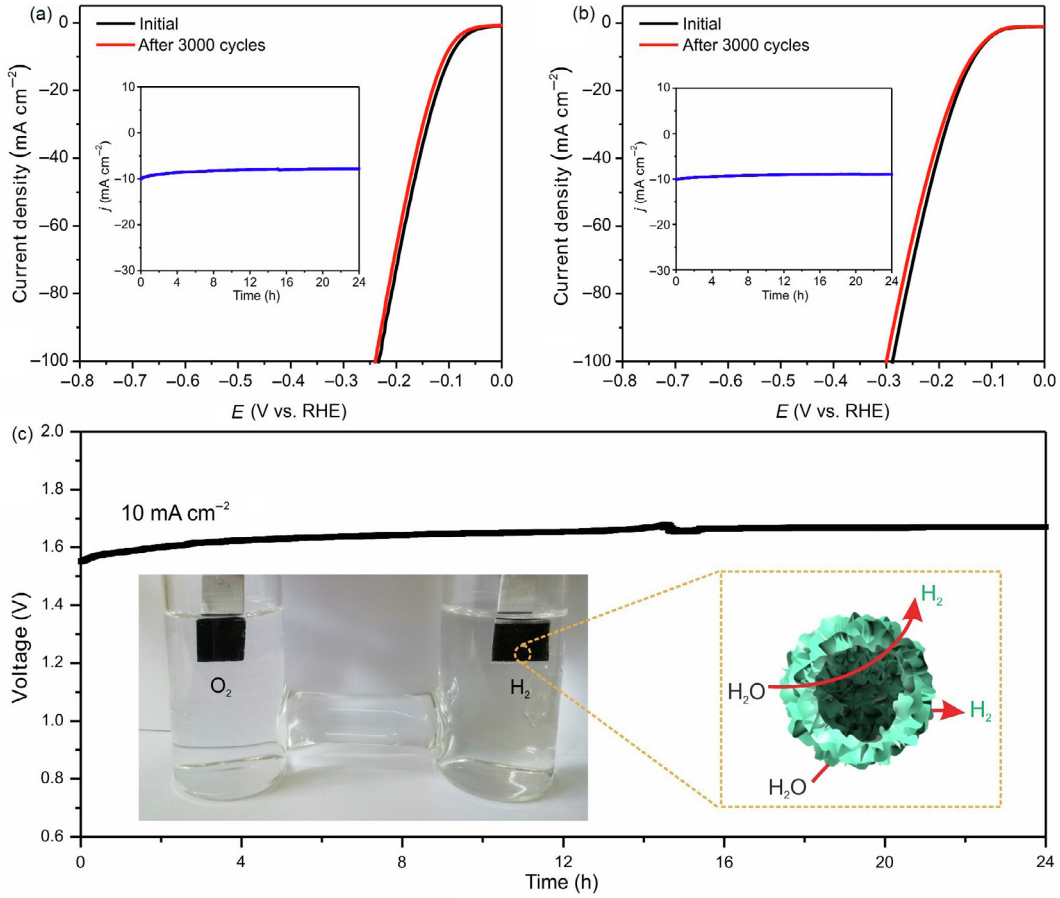

Fig. 5. (Color online) Polarization curves of NiCoP-150 initially and after 3000 CV cycles in 0.5 mol L^{-1} H_2SO_4 (a) and 1 mol L^{-1} KOH (b) (inset: the chronoamperometry response of NiCoP-150 for 24 h); (c) the chronopotentiometry curve of the assembled two-electrode cell in 1 mol L^{-1} KOH solution (inset: photograph of the assembled two-electrode cell for overall water splitting and illustration of hydrogen evolution on NiCoP-150).

assembly ultrathin nanosheets were achieved. In contrast with the solid NiCoP nanospheres, the hollow NiCoP nanoflowers are applied as a more efficient HER electrocatalyst benefitting from the large exposed active surface and affluent mass diffusion routes, which afford the current density of 10 mA cm^{-2} at small overpotentials of 95 and 127 mV in 0.5 mol L^{-1} H_2SO_4 and 1.0 mol L^{-1} KOH solution, respectively. Simultaneously, the hollow NiCoP nanoflowers display sustainable stability more than 24 h (10 mA cm^{-2}) in both acidic and alkaline conditions. Combing with Ir/C as oxygen evolution catalyst, the assembled alkaline electrolytic cell possesses outstanding durability for water splitting. This facile self-template method is promisingly expected to synthesize other transition metal catalysts with high specific surface area and excellent electrocatalytic property derived from solid-state metal alkoxides.

Conflict of interest

The authors declare that they have no conflict of interest.

Acknowledgments

This work was supported by the National Natural Science Foundation of China (21573083), and the Fundamental Research Funds for the Central Universities (2019kfyRCPY100). The authors thank the Analytical and Testing Center of HUST for allowing use of its facilities.

Author contributions

Deli Wang provided the key guidanceto design this work. Xupo Liu accomplished the experiments and the origin manuscript. All authors discussed the experimental results and revised this paper carefully.

Appendix A. Supplementary materials

Supplementary materials to this article can be found online at https://doi.org/10.1016/j.scib.2019.09.014.

References

[1] Feng JX, Wu JQ, Tong YX, et al. Efficient hydrogen evolution on Cu nanodots-decorated Ni_3S_2 nanotubes by optimizing atomic hydrogen adsorption and desorption. J Am Chem Soc 2018;140:610–7.
[2] Cai S, Wang R, Yourey WM, et al. An efficient bifunctional electrocatalyst derived from layer-by-layer self-assembly of a three-dimensional porous Co-N-C@graphene. Sci Bull 2019;64:968–75.
[3] Zhang Q, Yang Z, Ling Y, et al. Improvement in stability of PtRu electrocatalyst by carbonization of in-situ polymerized polyaniline. Int J Hydrogen Energy 2018;43:12730–8.
[4] Shi Y, Zhang B. Recent advances in transition metal phosphide nanomaterials: synthesis and applications in hydrogen evolution reaction. Chem Soc Rev 2016;45:1529–41.
[5] Yu J, Li W-J, Zhang H, et al. Metallic $FePSe_3$ nanoparticles anchored on N-doped carbon framework for All-pH hydrogen evolution reaction. Nano Energy 2019;57:222–9.
[6] Wang Y, Kong B, Zhao D, et al. Strategies for developing transition metal phosphides as heterogeneous electrocatalysts for water splitting. Nano Today 2017;15:26–55.
[7] Wang Y, Chen L, Mao Z, et al. Controlled synthesis of single cobalt atom catalysts via a facile one-pot pyrolysis for efficient oxygen reduction and hydrogen evolution reactions. Sci Bull 2019;64:1095–102.
[8] Callejas JF, Read CG, Popczun EJ, et al. Nanostructured Co_2P electrocatalyst for the hydrogen evolution reaction and direct comparison with morphologically equivalent CoP. Chem Mater 2015;27:3769–74.
[9] Zhao Y, Fan G, Yang L, et al. Assembling Ni-Co phosphides/carbon hollow nanocages and nanosheets with carbon nanotubes into a hierarchical necklace-like nanohybrid for electrocatalytic oxygen evolution reaction. Nanoscale 2018;10:13555–64.
[10] Wu Z, Song M, Zhang Z, et al. Various strategies to tune the electrocatalytic performance of molybdenum phosphide supported on reduced graphene oxide for hydrogen evolution reaction. J Colloid Interface Sci 2019;536:638–45.
[11] Sun S, Sun Y, Zhou Y, et al. Shifting oxygen charge towards octahedral metal: a way to promote water oxidation on cobalt spinel oxides. Angew Chem Int Ed 2019;58:6042–7.
[12] Teng Y, Wang XD, Liao JF, et al. Atomically thin defect-rich Fe-Mn-O hybrid nanosheets as high efficient electrocatalyst for water oxidation. Adv Funct Mater 2018;28:1802463.
[13] Li X, Du X, Ma X, et al. CuO nanowire@Co_3O_4 ultrathin nanosheet core-shell arrays: an effective catalyst for oxygen evolution reaction. Electrochim Acta 2017;250:77–83.
[14] Wu Z, Wang J, Liu R, et al. Facile preparation of carbon sphere supported molybdenum compounds (P, C and S) as hydrogen evolution electrocatalysts in acid and alkaline electrolytes. Nano Energy 2017;32:511–9.
[15] Ling Y, Yang Z, Zhang Q, et al. A self-template synthesis of defect-rich WS_2 as a highly efficient electrocatalyst for the hydrogen evolution reaction. Chem Commun 2018;54:2631–4.
[16] Liu T, Li P, Yao N, et al. Self-sacrificial template-directed vapor-phase growth of MOF assemblies and surface vulcanization for efficient water splitting. Adv Mater 2019;31:1806672.
[17] Xie L, Qu F, Liu Z, et al. *In situ* formation of a 3D core/shell structured Ni_3N@Ni-Bi nanosheet array: an efficient non-noble-metal bifunctional electrocatalyst toward full water splitting under near-neutral conditions. J Mater Chem A 2017;5:7806–10.
[18] Konkena B, Masa J, Xia W, et al. MoSSe@reduced graphene oxide nanocomposite heterostructures as efficient and stable electrocatalysts for the hydrogen evolution reaction. Nano Energy 2016;29:46–53.
[19] Wu Z, Wang J, Xia K, et al. MoS_2-MoP heterostructured nanosheets on polymer-derived carbon as an electrocatalyst for hydrogen evolution reaction. J Mater Chem A 2018;6:616–22.
[20] Li S, Zhang G, Tu X, et al. Polycrystalline CoP/CoP_2 structures for efficient full water splitting. ChemElectroChem 2018;5:701–7.
[21] Su J, Zhou J, Wang L, et al. Synthesis and application of transition metal phosphides as electrocatalyst for water splitting. Sci Bull 2017;62:633–44.
[22] Liu T, Li P, Yao N, et al. CoP-doped MOF-based electrocatalyst for pH-universal hydrogen evolution reaction. Angew Chem Int Ed 2019;58:4679–84.
[23] Cai Z, Wu A, Yan H, et al. Hierarchical whisker-on-sheet NiCoP with adjustable surface structure for efficient hydrogen evolution reaction. Nanoscale 2018;10:7619–29.
[24] Surendran S, Shanmugapriya S, Sivanantham A, et al. Electrospun carbon nanofibers encapsulated with NiCoP: a multifunctional electrode for supercapattery and oxygen reduction, oxygen evolution, and hydrogen evolution reactions. Adv Energy Mater 2018;8:1800555.
[25] Yin Z, Zhu C, Li C, et al. Hierarchical nickel-cobalt phosphide yolk-shell spheres as highly active and stable bifunctional electrocatalysts for overall water splitting. Nanoscale 2016;8:19129–38.
[26] Du C, Yang L, Yang F, et al. Nest-like NiCoP for highly efficient overall water splitting. ACS Catal 2017;7:4131–7.
[27] Liu C, Zhang G, Yu L, et al. Oxygen doping to optimize atomic hydrogen binding energy on NiCoP for highly efficient hydrogen evolution. Small 2018;14:1800421.
[28] Hu E, Feng Y, Nai J, et al. Construction of hierarchical Ni-Co-P hollow nanobricks with oriented nanosheets for efficient overall water splitting. Energy Environ Sci 2018;11:872–80.
[29] Sun Y, Shen Z, Xin S, et al. Ultrafine Co-doped ZnO nanoparticles on reduced graphene oxide as an efficient electrocatalyst for oxygen reduction reaction. Electrochim Acta 2017;224:561–70.
[30] Zhao J, Liu Y, Fan M, et al. From solid-state metal alkoxides to nanostructured oxides: a precursor-directed synthetic route to functional inorganic nanomaterials. Inorg Chem Front 2015;2:198–212.
[31] Kaneti YV, Salunkhe RR, Septiani NLW, et al. General template-free strategy for fabricating mesoporous two-dimensional mixed oxide nanosheets via self-deconstruction/reconstruction of monodispersed metal glycerate nanospheres. J Mater Chem A 2018;6:5971–83.
[32] Guo X, Liang J, Wang L, et al. Synthesis of cobalte-glycerate hierarchical structure and their conversion into hierarchical CoP nanospheres for the hydrogen evolution reaction. Int J Hydrogen Energy 2018;43:2034–42.
[33] Zhao J, Zou Y, Zou X, et al. Self-template construction of hollow Co_3O_4 microspheres from porous ultrathin nanosheets and efficient noble metal-free water oxidation catalysts. Nanoscale 2014;6:7255–62.
[34] Yu L, Xia BY, Wang X, et al. General formation of M-MoS_3 (M = Co, Ni) hollow structures with enhanced electrocatalytic activity for hydrogen evolution. Adv Mater 2016;28:92–7.
[35] Yang M, Li Y, Yu Y, et al. Self-assembly of three-dimensional zinc-doped $NiCo_2O_4$ as efficient electrocatalysts for oxygen evolution reaction. Chemistry 2018;24:13002–8.
[36] Zhu T, Chen JS, Lou XW. Highly Efficient removal of organic dyes from waste water using hierarchical NiO spheres with high surface area. J Phys Chem C 2012;116:6873–8.
[37] Jiang X, Wang Y, Herricks T, et al. Ethylene glycol-mediated synthesis of metal oxide nanowires. J Mater Chem 2004;14:695–703.
[38] Ding L, Zhang K, Chen L, et al. Formation of three-dimensional hierarchical pompon-like cobalt phosphide hollow microspheres for asymmetric supercapacitor with improved energy density. Electrochim Acta 2019;299:62–71.

[39] Wang M, Jiang J, Ai L. Layered bimetallic iron-nickel alkoxide microspheres as high-performance electrocatalysts for oxygen evolution reaction in alkaline media. ACS Sustainable Chem Eng 2018;6:6117–25.
[40] Larcher D, Sudant G, Patrice R, et al. Some insights on the use of polyols-based metal alkoxides powders as precursors for tailored metal-oxides particles. Chem Mater 2003;15:3543–51.
[41] Trogadas P, Ramani V, Strasser P, et al. Hierarchically structured nanomaterials for electrochemical energy conversion. Angew Chem Int Ed 2016;55:122–48.
[42] Niu KY, Park J, Zheng H, et al. Revealing bismuth oxide hollow nanoparticle formation by the Kirkendall effect. Nano Lett 2013;13:5715–9.
[43] Yin Y, Rioux RM, Erdonmez CK, et al. Formation of Hollow nanocrystals through the nanoscal Kirkendall effect. Science 2004;304:711–4.
[44] Lee JH. Gas sensors using hierarchical and hollow oxide nanostructures: overview. Sens Actuators B Chem 2009;140:319–36.
[45] Wang W, Dahl M, Yin Y. Hollow nanocrystals through the nanoscale Kirkendall effect. Chem Mater 2012;25:1179–89.
[46] Tan C, Cao X, Wu XJ, et al. Recent advances in ultrathin two-dimensional nanomaterials. Chem Rev 2017;117:6225–331.
[47] Wu T, Pi M, Wang X, et al. Hierarchical cobalt poly-phosphide hollow spheres as highly active and stable electrocatalysts for hydrogen evolution over a wide pH range. Appl Surf Sci 2018;427:800–6.
[48] Yu J, Li Q, Li Y, et al. Ternary metal phosphide with triple-layered structure as a low-cost and efficient electrocatalyst for bifunctional water splitting. Adv Funct Mater 2016;26:7644–51.
[49] Yang F, Chen Y, Cheng G, et al. Ultrathin nitrogen-doped carbon coated with cop for efficient hydrogen evolution. ACS Catal 2017;7:3824–31.
[50] Huang H, Yu C, Yang J, et al. Strongly coupled architectures of cobalt phosphide nanoparticles assembled on graphene as bifunctional electrocatalysts for water splitting. ChemElectroChem 2016;3:719–25.
[51] Liu H, Peng X, Liu X, et al. Porous Mn-doped FeP/$Co_3(PO_4)_2$ nanosheets as efficient electrocatalysts for overall water splitting in a wide pH range. ChemSusChem 2019;12:1334–41.
[52] Liu H, Liu X, Mao Z, et al. Plasma-activated $Co_3(PO_4)_2$ nanosheet arrays with Co^{3+}-rich surfaces for overall water splitting. J Power Sources 2018;400:190–7.
[53] Liu Q, Tian J, Cui W, et al. Carbon nanotubes decorated with CoP nanocrystals: a highly active non-noble-metal nanohybrid electrocatalyst for hydrogen evolution. Angew Chem Int Ed 2014;53:6710–804.
[54] Tian X, Zhao P, Sheng W. Hydrogen evolution and oxidation: mechanistic studies and material advances. Adv Mater 2019;31:1808066.
[55] Yang F, Zhao Y, Du Y, et al. A monodisperse Rh_2P-based electrocatalyst for highly efficient and pH-universal hydrogen evolution reaction. Adv Energy Mater 2018;8:1703489.
[56] Men Y, Li P, Zhou J, et al. Tailoring the electronic structure of Co_2P by N doping for boosting hydrogen evolution reaction at all pH values. ACS Catal 2019;9:3744–52.

Xupo Liu is currently a Post-doctoral from School of Chemistry and Chemical Engineering, Huazhong University of Science and Technology. He obtained doctoral degree at China University of Geosciences. His research interests focused on the design and synthesis of non-noble metal catalysts and proton exchange membranes for water splitting and fuel cells.

Deli Wang received her Ph.D. degree from Wuhan University in 2008. And then she joined in Nanyang Technological University working as a research fellow for one year. She moved to Cornell University in 2009, joined in Energy Materials Center at Cornell (EMC^2) as a postdoctoral associate for three years. She is currently a Professor of School of Chemistry and Chemical Engineering, Huazhong University of Science & Technology (HUST). Her research interests mainly focused on nanomaterials for energy conversion and storage.